High-Voltage Breakdown and the Gunn Effect in GaAs/AlGaAs Nanoconstrictions

Rui Chen, Weilu Gao, Xuan Wang, Gregory R. Aizin, John Mikalopas, Takashi Arikawa, Koichiro Tanaka, David B. Eason, Gottfried Strasser, Junichiro Kono, and Jonathan P. Bird

***Abstract*—We demonstrate dramatic breakdown behavior in the current through GaAs/AlGaAs nanoconstrictions (NCs), and find that this exhibits multiple signatures characteristic of the Gunn effect. These include current fluctuations and hysteresis, and electroluminescence that are consistent with the formation of Gunn domains. An analytical model is developed to describe the current–voltage characteristics of the NCs prior to the onset of the breakdown, and reveals the conduction through them to be barrier limited under low bias. A comparison of the results of these calculations with experiment furthermore suggests that the Gunn effect in these devices is triggered, once the phenomenon of drain-induced barrier lowering becomes sufficiently developed to support the injection of large numbers of electrons into the NC. Our paper, therefore, demonstrates how the Gunn effect may be manipulated through nanoscale tailoring of semiconductors, a result that may have implications for the development of solid-state terahertz technology.**

***Index Terms*— Gunn effect, nano-constrictions, nonequilibrium transport, terahertz devices.**

I. Introduction

NONEQUILIBRIUM phenomena in semiconductors have long provided fertile ground for the development of active electronic and photonic devices, with semiconductor lasers, photovoltaic cells, and light-emitting diodes providing just a few examples of such technologies. Enabling the realization of these, and other, semiconductor technologies are the fundamental modifications to carrier transport that arise under high electric fields, phenomena including [1]: saturation or overshoot of the drift-velocity; impact ionization and associated current avalanching; stimulated phonon emission, and; real- and *k*-space transfer of electrons. One of the key processes that embody the role of many of these phenomena is the Gunn effect that is exhibited by semiconductors such as GaAs and InP. In these materials, the scattering of electrons between different conduction-band valleys at high electric fields gives rise to velocity overshoot, the emergence of which is accompanied by the formation of inhomogeneous electric-field domains that ultimately are responsible for impact ionization and current avalanching [2]–[7]. Some 50 years on from its discovery, the Gunn effect continues to play an important role in microwave technology, by allowing the realization of versatile, high-power, microwave sources.

Nanoscale structuring of semiconductors offers an effective means to manipulate nonlinear carrier phenomena, with associated implications for the development of new device concepts. Large electric fields (>kV/cm) may be established by applying even modest voltages to such structures, while current flow may be restricted on a scale comparable to that associated with the essential carrier-scattering mechanisms. In both resonant tunneling diodes and ballistic hot-electron transistors, for example, operation relies on the capacity to manipulate carrier tunneling on distances shorter than the inelastic electron–phonon scattering length [8]. In quantum-cascade lasers, in contrast, optical-phonon emission is utilized to manipulate the relative populations of the different states involved in lasing, and to thereby provide a sustained scheme for operation [9].

While the Gunn effect has been studied more or less continuously since its discovery, and now provides the basis for mature microwave technology, the manifestations of this phenomenon in nanostructured devices have not been widely investigated to date. This issue is potentially one of considerable significance, however, with implications for the development of terahertz (THz) sources [10]–[16]. Although the present work does not address these proposals directly, it nonetheless represents an important step forward by demonstrating the manifestations of the Gunn effect in the current–voltage characteristics of semiconductor nanoconstrictions (NCs).

In this report, we discuss how the occurrence of the Gunn effect in semiconductor NCs gives rise to dramatic breakdown behavior, in which the onset of impact ionization is signaled by sharp discontinuities in the current through the device. In the study of its manifestations in bulk semiconductors, the Gunn effect is known to give rise to several characteristic signatures.

Manuscript received October 29, 2014; accepted March 17, 2015. Date of publication March 20, 2015; date of current version May 6, 2015. The review of this paper was arranged by Associate Editor Y.-H. Cho. This work was supported by the National Science Foundation under Award OISE0968405.

R. Chen, D. B. Eason, and J. P. Bird are with the Department of Electrical Engineering, University of Buffalo, Buffalo, NY 14260 USA (e-mail: rchen8@buffalo.edu; dbeason@buffalo.edu; jbird@buffalo.edu).

W. Gao and J. Kono are with the Department of Electrical and Computer Engineering, Rice UniversityHouston, TX 77005 USA (e-mail: weilu.gao@rice.edu; kono@rice.edu).

X. Wang was with the Department of Electrical and Computer Engineering, Rice University, Houston, TX 77005 USA. He is now with the Institute of Physics, Chinese Academy of Sciences, Beijing, 100190 China (e-mail: xw@iphy.ac.cn).

G. R. Aizin and J. Mikalopas are with the Department of Physical Sciences, Kingsborough College, City University of New York, Brooklyn, NY 11235 USA (e-mail: Y-Gregory.Aizin@kbcc.cuny.edu; John.Mikalopas@kbcc.cuny.edu).

T. Arikawa and K. Tanaka are with the Department of Physics, Kyoto University, Sakyo Kyoto 606-8502 Japan (e-mail: arikawa@scphys.kyoto-u.ac.jp; tanaka-g@icems.kyoto-u.ac.jp).

G. Strasser is with the Center for Micro and Nanostructures and the Institute for Solid State Electronics, Vienna University of Technology, Vienna 1040 Austria (e-mail: gottfried.strasser@tuwien.ac.at).

Color versions of one or more of the figures in this paper are available online at http://ieeexplore.ieee.org.

Digital Object Identifier 10.1109/TNANO.2015.2414902

These include: (1) current saturation arising from velocity overshoot [4]–[6]; (2) strongly-enhanced noise (and self-sustained current oscillations) induced by high-field domains [1], [3], [17], [18] and; (3) Electro-luminescence (EL) due to recombination of electrons and holes created by impact ionization within the domains [17], [19]–[22]. We demonstrate all of these features in the operation of GaAs-based NCs, thereby providing strong evidence that the Gunn effect may indeed be induced in such structures. While the present work provides only a first step in this direction, it suggests that observation of the Gunn effect in suitable NCs may eventually offer a means for both sourcing [10]–[16] and sensing [23]–[26] THz signals.

II. Experimental Methods

Etched NCs with various dimensions were realized in GaAs/AlGaAs heterojunctions. As illustrated in Fig. 1(a), the length and width of these structures was around a few hundred nanometers. The composition of the heterojunction used in these devices is shown in Fig. 1(b). The doping of the AlGaAs layer (with Si, at a concentration of $6.8 \times 10^{17}\,\mathrm{cm}^{-3}$) resulted in the formation of a two-dimensional electron gas (2-DEG), residing in the potential well formed at the heterointerface. Room-temperature carrier density and low-field mobility of this 2-DEG were $3 \times 10^{11}\,\mathrm{cm}^{-2}$ and 8000 cm^2/Vs, respectively, with a corresponding mean-free path of 70 nm. For measurements of their dc electrical characteristics, fabricated devices were wire-bonded into a chip carrier and mounted on the cold end of a simple dipping cryostat with heated stage. Unless stated otherwise, measurements reported here were obtained with the samples in the dark at room temperature. EL studies were performed under the same conditions, with the emitted light being collected by a multi-mode fiber. Its spectral content was analyzed with a grating spectrometer, equipped with a CCD camera operated at 77 K. By integrating this spectral information, the total EL intensity could thus be obtained.

III. Experimental Results

Close to zero bias, the NCs were pinched off due to Fermi-level pinning at their etched surfaces (see appendix), and several volts of applied bias were needed to "open" them. This is demonstrated in the upper-left panel of Fig. 1(c), in which we show measured current–voltage ($I_d - V_d$) characteristics for three different NCs. Each exhibits a clear threshold for the onset of current, at a voltage whose magnitude increases as the constriction width is reduced from 350 to 130 nm. These feature are captured by a theoretical model (see appendix) whose results are presented in the upper-right panel of Fig. 1(c). The essential feature of this model is the presence of a potential barrier within the NC, arising from the Fermi-level pinning. As the voltage induces a lowering of this barrier [25] a non-zero current may begin to flow, similar to the process of drain-induced barrier lowering (DIBL) in MOSFETs [27].

Comparing the current variations plotted in the upper two panels of Fig. 1(c), we see that our model accounts well for the behavior found in experiment. In our calculations of the 300-nm wide structure, I_d increases quickly beyond $|V_d| \tilde{}\, 0.4$ V before eventually saturating once $|V_d| > \tilde{}\, 1.5$ V. The saturation

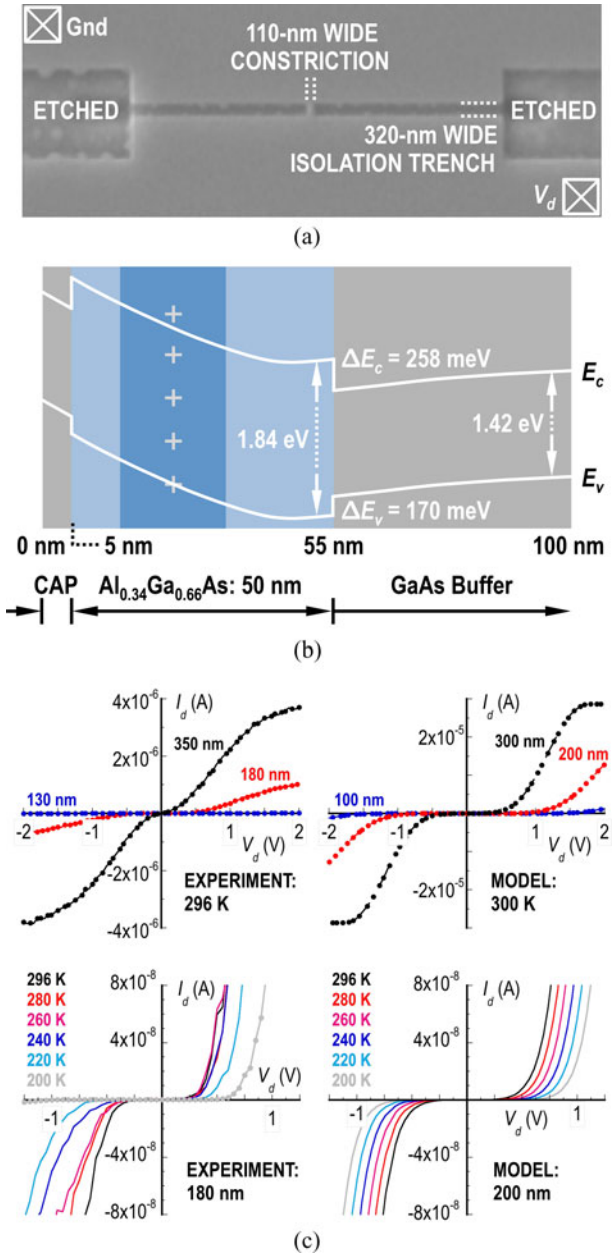

Fig. 1. (a) Electron micrograph of an etched GaAs/AlGaAs NC. (b) Layer structure of the heterojunction used here. The 20-nm thick dark-blue layer represents doped AlGaAs, which is separated from undoped GaAs (gray) by a 20-nm thick AlGaAs (light-blue) spacer. White lines denote the variations of the band edges (E_c and E_v) obtained from a self-consistent Poisson solver. (c) Upper-left: $I_d - V_d$ curves measured for NCs of indicated widths. In each device, constriction length was ~300 nm. Upper-right: $I_d - V_d$ curves computed for indicated widths. Lower-left: $I_d - V_d$ curves measured for the 180-nm NC at different temperatures. Lower-right: corresponding calculations for a 200-nm constriction.

arises when DIBL lowers the channel barrier so that it no longer limits transport (see appendix). The saturation is reproduced experimentally for the 350-nm constriction, and its approach is also apparent for the 180-nm device. In this latter case, the saturation is pushed to higher $|V_d|$, reflecting the presence of a larger barrier (see appendix). At the same time, the overall current level is reduced due to the narrower NC width. This trend is even more apparent for the 130-nm constriction, for which I_{d} is completely quenched over the entire range of V_d.

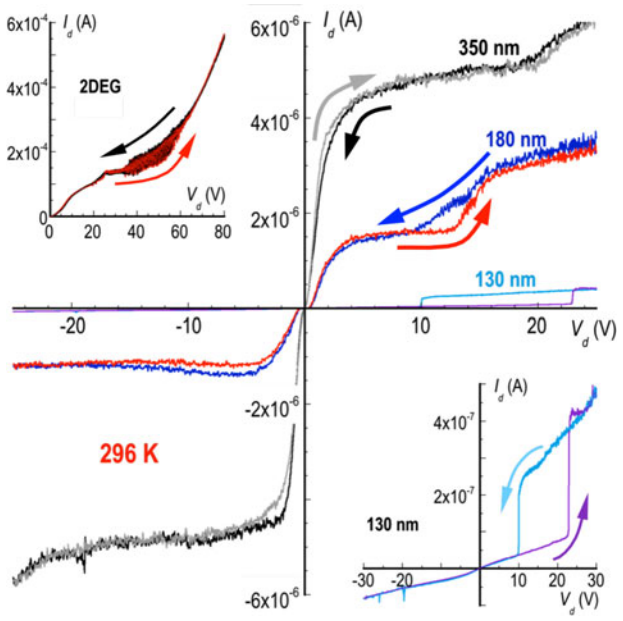

Fig. 2. Main panel: $I_d - V_d$ characteristics of the three NCs measured under strong nonequilibrium at 296 K. Upper inset: $I_d - V_d$ characteristics of 2-DEG measured at 296 K. Lower inset: expanded view of $I_d - V_d$ characteristic of the 130-nm constriction from the main panel. Colored arrows in the various panels indicate the direction of the voltage sweeps for each structure.

In the lower-left panel of Fig. 1(c), we show measured $I_d - V_d$ curves for the 180-nm NC for temperatures from 200 to 296 K. Consistent [28] with the barrier-limited transport at small V_d, the voltage required for the onset of current increases to larger $|V_{\rm d}|$ at lower temperatures, behavior that is also reproduced in our calculations (see Fig. 1(c), lower-right panel). Such agreement provides further confidence that, prior to the onset of strongly-nonequilibrium transport, we correctly identify the mechanisms governing the electrical characteristics of the NCs.

Turning to the behavior observed under strong nonequilibrium, in the main panel of Fig. 2 we demonstrate several manifestations of the Gunn effect in the three NCs when they are subjected to large biases. To understand this behavior we refer to the upper-left inset of the figure, where we show the $I_d - V_d$ characteristic of the unetched 2-DEG at voltages up to 80 V. Sweeping voltage up and down yields similar characteristics, with several features typical of the Gunn effect. The first is current saturation [4]–[6], which onsets around 20 V and which serves as the precursor to the second feature, a region ($35 \leq V_d \leq 65$V) of strongly-enhanced noise [17], [18].

The Gunn-related features exhibited by the 2-DEG are significantly modified in the NCs, as we show in the main panel of Fig. 2. Starting with the widest (350-nm) constriction, $I_{\rm d}$ increases rapidly for a small increase of V_d, before eventually saturating once $|V_d| \sim 4$ V. This saturation is attributed to DIBL, rather than the Gunn effect, however, since it is also found in our calculations that do *not* include any inter-valley transfer (see appendix). Simultaneous with the approach to saturation, a noticeable increase in current noise occurs. Such behavior *is* consistent with the Gunn effect, usually being associated with a stochastic motion of high-field domains between the contacts of the device. The close correlation between the approach to saturation and the onset of this noise suggests that the Gunn effect in the NCs occurs more or less simultaneous with the full lowering of their barrier. Prior to this, the electron density inside the constriction is likely too small to initiate the Gunn mechanism, which seems to be triggered instead once DIBL allows sufficient numbers of electrons to be injected into the high-field region formed by the NC.

Further reduction of the NC width results in the appearance of new features (see Fig. 2) in the $I_d - V_d$ curves. The first is an enhanced noise level at high bias, at least compared to the 350-nm constriction, indicating that Gunn instabilities have a much more pronounced effect on the $I_d - V_d$ curve of the narrower constrictions. Secondly, the $I_d - V_d$ curve of the narrowest constriction is strongly asymmetric, exhibiting "diode-like" behavior. This results from the well-known asymmetry of mesoscopic barriers to reversal of their bias voltage [28]. Finally, we observe breakdown in the current through the device, arising from avalanching-type behavior that is accompanied by the presence of pronounced hysteresis. While this breakdown is absent in our measurements of unpatterned 2-DEGs, its effect becomes more dramatic as the NC width is reduce (compare the behavior of the 180-nm NC in Fig. 2 and the 130-nm structure in the lower inset). The breakdown defines a region of pronounced hysteresis as the bias voltage is swept, in which the current through the constriction essentially turns on or off at very different voltages. In the data for the narrowest channel, the modulation of current produced by these features is as large as 400%, while the range of the hysteresis spans some 12 V. While hysteresis is known from studies of the Gunn effect in bulk semiconductors, where it is a result of instabilities produced by impact ionization [17], [18], the fact that it is accompanied by such a dramatic breakdown in the current means that its effect is greatly enhanced here.

In Fig. 3, we plot $I_d - V_d$ curves for the 130-nm NC, which shows the most pronounced breakdown behavior, at temperatures from 230 to 296 K. Decrease of temperature causes significant shrinkage in the area of the hysteresis loop. This arises predominantly from a change in the structure of the up sweeps, whose current discontinuity shifts from 23 V at 296 K, to around 9 V at 230 K. Such temperature dependence is typically associated with impact ionization, a natural consequence of forming high-field domains in the Gunn effect. As the temperature is lowered and the mean-free path increases the ionization onsets at lower voltages [29], [30]. As we indicate in the upper inset to Fig. 3, 2-DEG mobility increases by a factor of $\sim$2 when the temperature is lowered over this range, consistent with the observed shift of the up-sweep current discontinuity. This therefore supports an interpretation in terms of impact ionization. Finally, we note that the overall tendency for the current to decrease with reduction of temperature is consistent with the influence of barrier-limited thermal activation in the structure.

The strongest evidence that the breakdown behavior arises from impact ionization within Gunn domains is provided by EL (see Fig. 4) from the devices for a wide range of voltages. EL is a natural byproduct of impact ionization, arising from the recombination of excess electrons and holes generated by the ionization. In the main panel of Fig. 4(a), we plot measured EL intensity as a function of V_d for the 180-nm NC. In the inset to

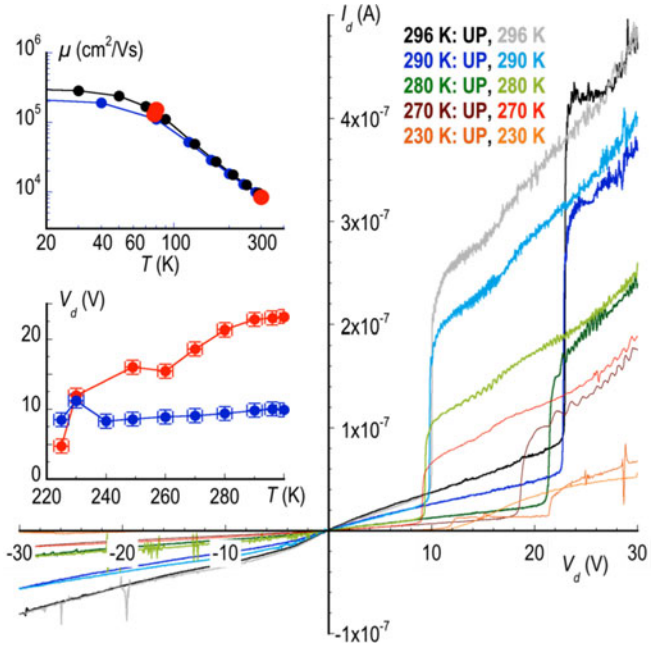

Fig. 3. Main panel: $I_d - V_d$ characteristic of 130-nm wide NC measured at indicated temperatures. At each temperature, darker (lighter) color denotes sweeping from –30 to +30 V (+30 to –30 V). Upper inset: 2-DEG mobility versus temperature. Black and blue filled circles: two other heterostructures similar to that used here. Red filled circles: 2-DEG used in this study. Lower inset: Position of discrete current jumps that define the hysteresis loops in the $I_d - V_d$ curves. Red (blue) data: sweeping from negative to positive (positive to negative) voltage.

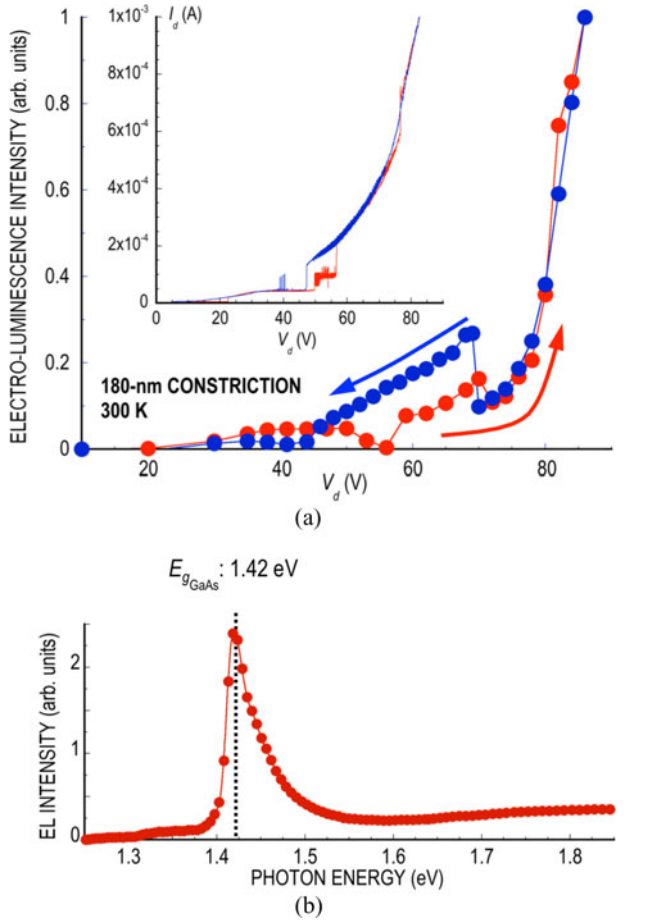

Fig. 4. (a) EL measured for the 180-nm constriction as a function of V_d. Red (blue) data: sweeping voltage up from (down towards) 0 V. Inset: $I_d - V_d$ curve for this device. Colored curves correspond to the same sweep directions as the main panel. (b) Room-temperature EL spectrum obtained for the 180-nm NC (at $V_d = 90$ V).

Fig. 4(a) we show the $I_d - V_d$ characteristic of the NC, which exhibits the various features that we have discussed already. (The wide voltage sweep used here was required to generate a sufficiently large EL signal.) By comparing the behaviors in the main panel and the inset of Fig. 4(a) we see that EL is observed over the entire range of Gunn behavior ($\sim 20 - 90$V). The spectral content of the EL is plotted for a representative bias of 90 V in Fig. 4(b), where we see a sharp cut-off below the GaAs bandgap ($E_{g_{GaAs}} = 1.42$ eV). This observation is clearly consistent with a process in which high-field domains cause impact ionization and EL in the GaAs 2-DEG.

IV. Discussion

The collective results described above reveal the following picture of nonequilibrium transport in the NCs. The essential feature of these structures is a strong depletion of carriers near their etched surfaces, caused by Fermi-level pinning at surface electron states. Since the spatial scale of this depletion exceeds the size of the NC, a significant potential barrier is formed within it (see appendix). This barrier strongly suppresses current flow at low biases, even in measurements performed at room temperature. With the application of sufficient bias, however, the NC opens once DIBL allows electrons to be injected into it in large numbers. With the DIBL fully developed, a bias voltage of even just a few volts—dropped across the submicron-length NCs—should be sufficient to induce the Gunn effect [2]–[6]. This is consistent with our observation that the enhanced current noise, attributed to Gunn-domain propagation, onsets as the NCs open [11].

The strongly-hysteretic breakdown exhibited by the NCs is related to impact ionization, which should onset once the maximum electric-field strength within the traveling domains exceeds that required for this process. The ionization increases the electron density within the NC, causing a further increase of the electric field within the domain [4]–[6]. It is this positive feedback that initiates the avalanche-like increase of current seen in the NCs. It has long been known from experimental [17], [18] and theoretical [4], [31] studies of bulk semiconductors that this behavior yields hysteretic $I_d - V_d$ curves. The behavior reported here, however, is far more dramatic, since the narrow constrictions strongly limit current flow to a low level near zero bias, allowing the onset of the impact ionization to produce a much larger relative current change than in bulk. As the electron mean-free path increases with decrease of temperature, the electric field needed to trigger the ionization should decrease towards zero, just as we observe (see Fig. 3, lower inset). At sufficiently low temperatures, electron transfer through the submicron NCs may approach the ballistic limit. The rapid quenching of the hysteresis with decreasing temperature (see

Fig. 3) may be connected to such a transition, although this aspect of our data is not well understood at present.

The mechanism for the current instabilities that we discuss appears to be quite different to that explored in earlier studies of nonequilibrium transport in heterostructure devices [32]–[37]. Among these works, significant effort focused on the realization of instabilities in vertical (tunneling) transport, where the key phenomenon was found to be thermionically-driven real-space transfer of hot electrons between different layers of the heterostructure [32]–[36]. While we cannot rule out the possibility that real-space transfer may also arise in our devices, it does not appear to be the dominant mechanism responsible for the observed instabilities. We point here to our EL studies, which show a strong signature arising from band-to-band recombination in the GaAs layer. This tends to support the idea that the driving mechanism for the EL is indeed inter-valley transfer associated with the Gunn effect. In Ref. [37], instabilities were reported in planar structures more similar to the NCs considered here. That work focused on double point contact devices, however, in which *S*-shaped current-voltage characteristics were argued to result from hot-carrier thermal runaway in a region of 2-DEG located between the point contacts. As a conduction-band process, however, it is not clear how this would generate the EL that we observe.

V. Conclusion

In conclusion, we have demonstrated dramatic current breakdown in GaAs/AlGaAs NCs subjected to strong biasing, and have shown that this reveals multiple signatures characteristic of the Gunn effect. Current saturation in these structures is associated with DIBL, which allows the injection of carriers into their initially-depleted channels, acting as the trigger for the Gunn effect. The saturation is accompanied by the emergence of low-frequency noise and by EL, both of which are consistent with the presence of high-field domains. Although not the focus of this work, our demonstrations of the Gunn effect in these structures may eventually allow their use in THz technology. Theoretical work suggests, for example, the possibility of utilizing the Gunn effect in nanoscale diodes to source THz signals [10]–[16]. At the same time, the strongly nonlinear nature of the current associated with the high-field breakdown may be useful for rectification-based detector of such radiation. Before these goals can be demonstrated, however, it is necessary to establish the nature of the high-field domains in these devices, and to explicitly prove the presence of THz oscillations arising from the Gunn effect. While these tasks are certainly challenging, the ability to use NCs as compact THz sources would represent a significant advance.

Appendix

Low-Field Transport Through Etched NCs: Theoretical Modeling

In the etched GaAs NCs that we study, the Fermi level is pinned near midgap due to the influence of surface states that form at the exposed NC walls. The pinning results in the formation of depletion regions near these walls, as the energy bands

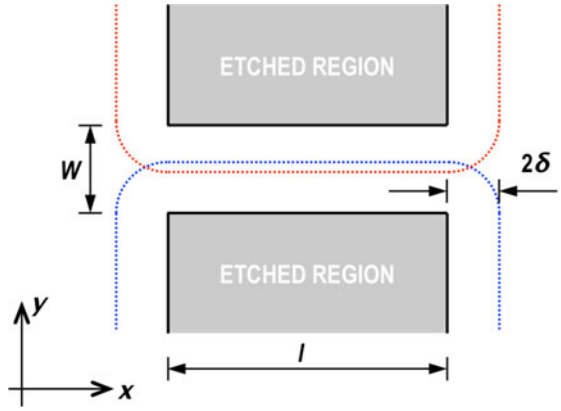

Fig. 5. Schematic illustration of the NC geometry, indicating the important length scales utilized in our discussion, as well as the definition of our coordinate axes. The red and blue dotted lines indicate the range of the depletion regions generated at the opposite etched surfaces of the NC.

of the semiconductor bend to accommodate the mid-gap pinning. In narrow NCs, the depletion regions formed at opposite walls overlap, producing a potential barrier in the channel. At low source–drain biases, this barrier blocks electron transport so that the channel is effectively pinched off. To estimate the height of this potential barrier we use a model originally developed for quasi-one-dimensional channels formed by negative biasing of split metal gate [38]. In this model, the gates are positioned above a 2-DEG, at the semiconductor-vacuum boundary. With sufficiently-large negative gate voltage ($V_{\rm g}$) applied, the 2-DEG in the gap between the gates can completely depleted. In [38], the electrostatic potential variation across the depleted electron channel was calculated, using the methods of the theory of analytical functions. As discussed in [39], this result can be generalized to etched NCs, such as those of interest here, by replacing the gate voltage in an *ad hoc* manner, with half the bandgap ($E_{\rm g}$) of the host semiconductor (assuming that the Fermi-level is pinned at $E_{\rm g}/2$). For a 2-DEG embedded in a medium with dielectric permittivity ε we arrive at the following expression [26]:

$$V(y) = \frac{E_g}{2} - \frac{en_0}{2\varepsilon\varepsilon_0}\sqrt{\left(\frac{W}{2}\right)^2 - y^2}, \tag{1}$$

where W is the physical (etched) width of the NC and n_0 is the equilibrium density of the unetched 2-DEG. Here, the y-axis is defined as the direction across the NC width, while the x-axis runs along the length of the constriction. These and other important length scales are defined in Fig. 5.

It follows from (1) that the height of the potential barrier seen by electrons traveling along the x-axis is:

$$V_0 = \frac{E_g}{2} - \frac{en_0 W}{4\varepsilon\varepsilon_0}. \tag{2}$$

For the GaAs-based NCs of interest here, we have $E_g = 1.412$ eV and $\varepsilon = 13$. To make direct connection to the results of experiment, we then used $n_0 = 3 \times 10^{15}\,\mathrm{m}^{-2}$ to compute the barrier heights quoted here.

With a voltage ($V_{\rm d}$) applied across the NC its barrier decreases due to the DIBL effect. To describe this effect quantitatively we

have developed a simple analytical model in which we assume that the electrostatic potential varies in a step-like manner at the entrance and exit to the NC. At $V_{\rm d} = 0$, this variation can be described as follows:

$$V(x) = V_0 P(x),$$
$$P(x) = \frac{1}{1+e^{-\frac{x+l/2}{\delta}}} + \frac{1}{1+e^{\frac{x-l/2}{\delta}}} - 1. \tag{3}$$

Here, l is the physical length of the NC, 2δ is the size of a transition region between the unetched regions of 2-DEG and the NC (see Fig. 5), and V_0 is defined in (2). The potential profile $V(x)$ is shown in Fig. 6(a), for a NC with $l/2\delta = 10$ and at $V_{\rm d} = 0$. The potential drop at the entrance and exit to the NC is taken here to be symmetric, which, as we have seen, need not be the case in experiment. Nonetheless, the assumption of a symmetric channel should suffice for the discussion of the DIBL effect. At non-zero $V_{\rm d}$, the potential difference between the source and the drain will be dropped mostly across the pinched off NC, because of its very high resistance compared to that of the unetched 2-DEG. Therefore, the electric field ($E_{\rm b}$) generated by the applied voltage V_d is finite within the NC only and vanishes in the adjacent unetched 2-DEG regions. We assume that this field can be modeled by the function $P(x)$ from Eq. (3) as:

$$E_b = -\frac{\partial V_1(x)}{\partial x} = AP(x), \tag{4}$$

where $V_1(x)$ is the electrostatic potential induced by the applied bias and the constant A can be found from the boundary condition:

$$\int_{-\infty}^{\infty} \frac{\partial V_1}{\partial x} dx = -V_d, \tag{5}$$

which yields $A = V_d/l$. Integration of (4) with $V_1(x = \infty) = 0$ then gives:

$$V_1(x) = -\frac{V_d \delta}{l} \ln\left(\frac{1+e^{-\frac{x+l/2}{\delta}}}{1+e^{-\frac{x-l/2}{\delta}}}\right). \tag{6}$$

The total potential within the NC is:

$$V_{\rm tot}(x) = V(x) + V_1(x). \tag{7}$$

This potential is shown in Fig. 6(b) at $V_d/V_0 = 0.8$. The potential barrier H in the biased NC depends on V_d and is determined as:

$$H(V_d) = V_{\rm tot}(x_m) - V_d. \tag{8}$$

Here, x_m is the point in the channel where $V_{\rm tot}$ takes its maximum value. When V_d increases, the barrier height defined in (8) decreases in the manner illustrated in Fig. 6(c). It is this phenomenon of barrier lowering that is the DIBL effect.

To calculate the current–voltage characteristics shown in Fig. 1(c), we made use of the standard expression for the thermally-activated current due to ballistically-transmitted carriers:

$$I(V_d, T) = \frac{eW}{\pi h} \int_0^{\infty} [f(E) - f(E+V_d)] \left(\int_{-\infty}^{\infty} P(E, k_y)\, dk_y\right) dE. \tag{9}$$

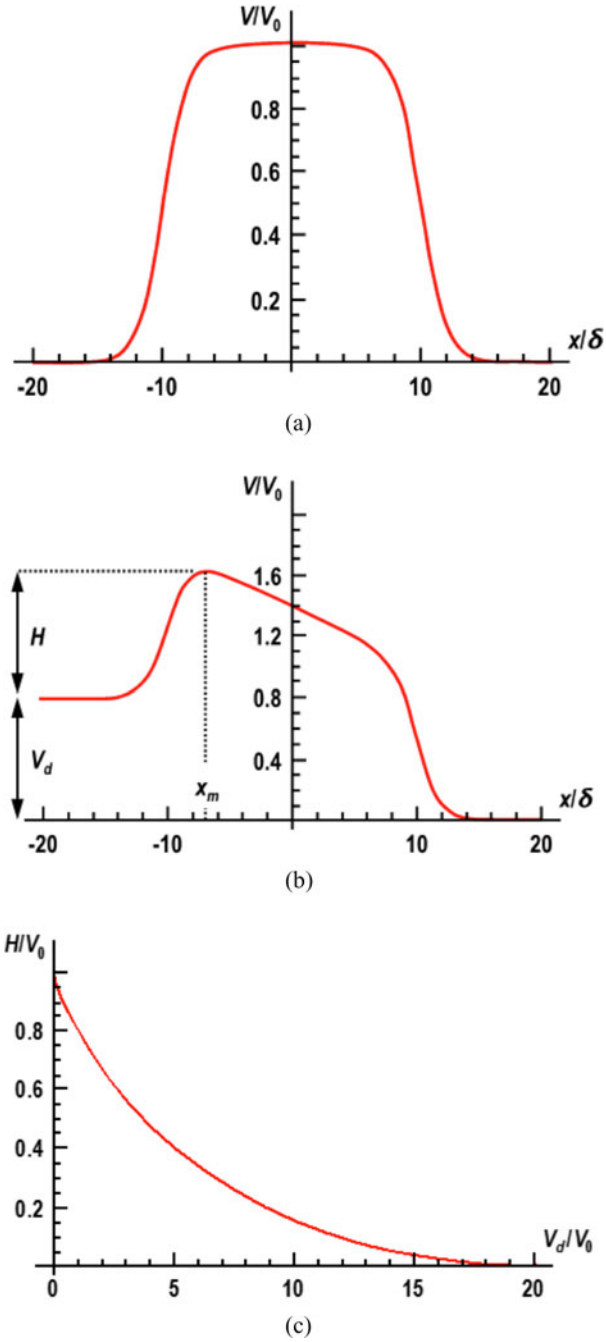

Fig. 6. (a) Electrostatic potential profile in the NC at $V_d = 0$. (b) The same as in (a) but at $V_d = 0.8V_0$. (c) The electrostatic barrier height as a function of V_d.

Here $f(E)$ is Fermi distribution function, calculated at the specific temperature (T) of interest. $P(E, k_{\rm y})$ is the probability for an electron with energy E and transverse momentum k_y to be transmitted across the barrier. Due to the relatively-long channel length in these devices we neglect the influence of tunneling, so that $P(E, k_{\rm y}) = 1$ (0) when $E > \mu + H (E < \mu + H)$ where μ is the chemical potential. In the calculations shown in Fig. 1(c), we estimated the transition length 2δ by considering it to be equal to the depletion length ($\sim$100 nm) at the edge of an unetched 2-DEG, while using a value of $l = 300$ nm.

REFERENCES

[1] S. M. Sze and K. K. Ng, *Physics of Semiconductor Devices*, 3rd ed. Hoboken, NJ, USA: Wiley, 2007.

[2] J. B. Gunn, "Microwave oscillations of current in III-V semiconductors," *Solid-State Commun.*, vol. 1, no. 4, pp. 88–91, Sep. 1963.

[3] J. S. Heeks, "Some properties of the moving high-field domain in Gunn effect devices," *IEEE Trans. Electron Dev.*, vol. ED-13, no. 1, pp. 68–79, Jan. 1966.

[4] M. E. Levinshtein and M. S. Shur, "The Gunn effect (review)," *Soviet Phys. Semicond.*, vol. 5, no. 9, pp. 1561–1588, Mar. 1972.

[5] G. S. Hobson, *The Gunn Effect*, London, U.K.: Clarendon, 1974.

[6] M. P. Shaw, H. L. Grubin, and P. R. Solomon, *The Gunn-Hilsum Effect*. New York, NY, USA: Academic, 1979.

[7] H. L. Grubin, D. K. Ferry, and K. R. Gleason, "Spontaneous oscillations in gallium arsenide field effect transistors," *Solid State Electron.*, vol. 23, no. 2, pp. 157–172, Feb. 1980.

[8] J. Smoliner, D. Rakoczy, and M. Kast, "Hot electron spectroscopy and microscopy," *Rep. Prog. Phys.*, vol. 67, no. 10, pp. 1863–1914, Aug. 2004.

[9] B. S. Williams, "Terahertz quantum-cascade lasers," *Nature Photon.*, vol. 1, pp. 517–525, Sep. 2007.

[10] K. Y. Xu, G. Wang, and A. M. Song, "Gunn oscillations in a self-switching nanodiode," *Appl. Phys. Lett.*, vol. 93, no. 23, pp. 233506-1–233506-3, Dec. 2008.

[11] A. Iñiguez-de-la-Torre, I. Iñiguez-de-la-Torre, J. Mateos, and T. González, "Correlation between low-frequency current-noise enhancement and high-frequency oscillations in GaN-based planar nanodiodes: A Monte Carlo study," *Appl. Phys. Lett.*, vol. 99, no. 6, pp. 062109-1–062109-3, Aug. 2011.

[12] A. Iñiguez-de-la-Torre, I. Iñiguez-de-la-Torre, J. Mateos, T. González, P. Sangaré, M. Faucher, B. Grimbert, V. Brandli, G. Ducournau, and C. Gaquière, "Searching for THz Gunn oscillations in GaN planar nanodiodes," *J. Appl. Phys.*, vol. 111, no. 11, pp. 113705-1–113705-9, Jun. 2012.

[13] P. Sangaré, G. Ducournau, B. Grimbert, V. Brandli, M. Faucher, C. Gaquière, A. Íñiguez-de-la-Torre, I. Íñiguez-de-la-Torre, J. F. Millithaler, J. Mateos, and T. González, "Experimental demonstration of direct terahertz detection at room-temperature in AlGaN/GaN asymmetric nanochannels," *J. Appl. Phys.*, vol. 113, no. 3, pp. 034305-1–034305-6, Jan. 2013.

[14] S. Garcia, I. Iñiguez-de-la-Torre, S. Pérez, J. Mateos, and T. González, "Numerical study of sub-millimeter Gunn oscillations in InP and GaN vertical diodes: Dependence on bias, doping, and length," *J. Appl. Phys.*, vol. 114, no. 7, pp. 074503-1–074503-9, Aug. 2013.

[15] K. Y. Xu, J. Li, J. W. Xiong, and G. Wang, "Mutual phase-locking of planar nano-oscillators," *AIP Adv.*, vol. 4, no. 6, pp. 067108-1–067108-8, Jun. 2014.

[16] A. Khalid, G. M. Dunn, R. F. Macpherson, S. Thoms, D. Macintyre, C. Li, M. J. Steer, V. Papageorgiou, I. G. Thayne, M. Kuball, C. H. Oxley, M. M. Bajo, A. Stephen, J. Glover, and D. R. S. Cumming, "Terahertz oscillations in an In0.53Ga0.47As submicron planar Gunn diode," *J. Appl. Phys.*, vol. 115, no. 11, pp. 114502-1–114502-6, Mar. 2014.

[17] S. G. Liu, "Infrared and microwave radiations associated with a current controlled instability in GaAs," *Appl. Phys. Lett.*, vol. 9, no. 2, pp. 79–81, Jul. 1966.

[18] P. D. Southgate, "Recombination processes following impact ionization by high field domains in gallium arsenide," *J. Appl. Phys.*, vol. 38, no. 12, pp. 4589–4595, Nov. 1967.

[19] H. P. Zappe and C. Moglestue, "Electroluminescence from Gunn domains in GaAs/AlGaAs heterostructure field effect transistors," *J. Appl. Phys.*, vol. 68, no. 5, pp. 2501–2503, Sep. 1990.

[20] E. Zanoni, L. Vendrame, P. Pavan, M. Manfredi, S. Bigliardi, R. Malik, and C. Canali, "Hot electron electroluminescence in AlGaAs/GaAs heterojunction bipolar transistors," *Appl. Phys. Lett.*, vol. 62, no. 4, pp. 402–404, Jan. 1993.

[21] F. Klappenberger, K. F. Renk, R. Summer, L. Keldysh, and B. Rieder, "Electric-field-induced reversible avalanche breakdown in a GaAs microcrystal due to cross band gap impact ionization," *Appl. Phys. Lett.*, vol. 83, no. 4, pp. 704–706, Jul. 2003.

[22] M. Montes Bajo, G. Dunn, A. Stephen, A. Khalid, D. R. S. Cumming, C. H. Oxley, J. Glover, and M. Kuball, "Impact ionisation electroluminescence in planar GaAs-based heterostructure Gunn diodes: Spatial distribution and impact of doping non-uniformities," *J. Appl. Phys.*, vol. 113, no. 12, pp. 124505-1–124505-6, Mar. 2013.

[23] S. A. Dayeh, D. Susac, K. L. Kavanagh, E. T. Yu, and D. Wang, "Field dependent transport properties in InAs nanowire field effect transistors," *Nano Lett.*, vol. 8, no. 10, pp. 3114–3119, Sep. 2008.

[24] C. Balocco, A. M. Song, M. Åberg, A. Forchel, T. González, J. Mateos, I. Maximov, M. Missous, A. A. Rezazadeh, J. Saijets, L. Samuelson, D. Wallin, K. Williams, L. Worschech, and H. Q. Xu, "Microwave detection at 110 GHz by nanowires with broken symmetry," *Nano Lett.*, vol. 5, no. 7, pp. 1423–1427, Jun. 2005.

[25] M. S. Vitiello, D. Coquillat, L. Viti, D. Ercolani, F. Teppe, A. Pitanti, F. Beltram, L. Sorba, W. Knap, and A. Tredicucci, "Room-temperature terahertz detectors based on semiconductor nanowire field-effect transistors," *Nano Lett.*, vol. 12, no. 1, pp. 96–101, Dec. 2011.

[26] R. Chen, J. W. Song, T. Y. Lin, G. R. Aizin, Y. Kawano, N. Aoki, Y. Ochiai, V. R. Whiteside, B. D. McCombe, D. Thomas, M. Einhorn, J. L. Reno, G. Strasser, and J. P. Bird, "Terahertz detection with nanoscale semiconductor rectifiers," *IEEE Sens. J.*, vol. 13, no. 1, pp. 24–30, Jan. 2013.

[27] Y. Tsividis, *Operational Modeling of the MOS Transistor*, 2nd ed. New York, NY, USA: Oxford Univ. Press, 1999.

[28] K. S. Novoselov, Yu. V. Dubrovskii, V. A. Sablikov, D. Yu. Ivanov, E. E. Vdovin, Yu. N. Khanin, V. A. Tulin, D. Esteve, and S. Beaumont, "Nonlinear electron transport in normally pinched-off quantum wire," *Europhys. Lett.*, vol. 52, no. 6, pp. 660–666, Mar. 2000.

[29] N. Dyakonova, A. Dickens, M. S. Shur, R. Gaska, and J. W. Yang, "Temperature dependence of impact ionization in AlGaN–GaN heterostructure field effect transistors," *Appl. Phys. Lett.*, vol. 72, no. 20, pp. 2562–2564, May 1998.

[30] H. Hirori, K. Shinokita, M. Shirai, S. Tani, Y. Kadoya, and K. Tanaka, "Extraordinary carrier multiplication gated by a picosecond electric field pulse," *Nature Commun.*, vol. 2, pp. 594-1–594-6, Dec. 2011.

[31] B. K. Ridley, "Specific negative resistance in solids," *Proc. Phys. Soc.*, vol. 82, no. 6, pp. 954–966, Dec. 1963.

[32] K. Hess, T. K. Higman, M. A. Emanuel, and J. J. Coleman, "New ultrafast switching mechanism in semiconductor heterostructures," *J. Appl. Phys.*, vol. 60, no. 10, pp. 3775–3777, Nov. 1986.

[33] T. K. Higman, J. M. Higman, M. A. Emanuel, K. Hess, and J. J. Coleman, "Theoretical and experimental analysis of the switching mechanism in heterostructure hot-electron diodes," *J. Appl. Phys.*, vol. 62, no. 4, pp. 1495–1499, Aug. 1987.

[34] M. A. Emanuel, T. K. Higman, J. M. Higman, J. M. Kolodzey, J. J. Coleman, and K. Hess, "Theoretical and experimental investigations of the heterostructure hot-electron diode," *Solid State Electron.*, vol. 31, nos. 3/4, pp. 589–592, Mar. 1988.

[35] D. Arnold, K. Hess, and G. J. Iafrate, "Electron transport in heterostructure hot-electron diodes," *Appl. Phys. Lett.*, vol. 53, no. 5, pp. 373–375, Aug. 1988.

[36] T. K. Higman, L. M. Miller, M. E. Favaro, M. A. Emanuel, K. Hess, and J. J. Coleman, "Room-temperature switching and negative differential resistance in the heterostructure hot-electron diode," *Appl. Phys. Lett.*, vol. 53, no. 17, pp. 1623–1625, Oct. 1988.

[37] J. C. Wu, M. N. Wybourne, C. Berven, S. M. Goodnick, and Doran D. Smith, "Negative differential conductance observed in a lateral double constriction device," *Appl. Phys. Lett.*, vol. 61, no. 20, pp. 2425–2427, Nov. 1992.

[38] L. I. Glazman and I. A. Larkin, "Lateral position control of an electron channel in a split-gate device," *Semicond. Sci. Technol.*, vol. 6, no. 1, pp. 32–35, Dec. 1991.

[39] D. B. Chklovskii, B. I. Shklovskii, and L. I. Glazman, "Electrostatics of edge channels," *Phys. Rev. B*, vol. 46, no. 7, pp. 4026–4034, Sep. 1992.

Author's photographs and biographies not available at the time of publication.